

# We are IntechOpen, the world's leading publisher of Open Access books Built by scientists, for scientists

6,900

Open access books available

185,000

International authors and editors

200M

Downloads

Our authors are among the

154

Countries delivered to

TOP 1%

most cited scientists

12.2%

Contributors from top 500 universities



WEB OF SCIENCE™

Selection of our books indexed in the Book Citation Index  
in Web of Science™ Core Collection (BKCI)

Interested in publishing with us?  
Contact [book.department@intechopen.com](mailto:book.department@intechopen.com)

Numbers displayed above are based on latest data collected.  
For more information visit [www.intechopen.com](http://www.intechopen.com)



---

# Artificial Neural Network-Genetic Algorithm Prediction of Heavy Metal Removal Using a Novel Plant-Based Biosorbent Banana Floret: Kinetic, Equilibrium, Thermodynamics and Desorption Studies

---

Clint Sutherland, Abeni Marcano and  
Beverly Chittoo

Additional information is available at the end of the chapter

<http://dx.doi.org/10.5772/intechopen.74398>

---

## Abstract

In this study, the biosorption performance of banana floret was assessed as a new biosorbent for the removal of Cu(II) ions (a model heavy metal) from aqueous solutions. Batch experiments were conducted to assess the effects of agitation, particle size, pH, temperature and initial concentration. Kinetic and equilibrium data were modeled, and mass transfer studies were conducted to elucidate the mechanisms of biosorption. Kinetic data were best simulated using the diffusion-chemisorption model while equilibrium data were best represented by the Sips isotherm. The dominant transport mechanism was attributed to intraparticle diffusion while the dominant attachment mechanism was chemical sorption. A predictive model was successfully developed using an artificial neural network (ANN) and optimized using a genetic algorithm (GA). The accuracy of the ANN-GA prediction was validated by laboratory experiments, which revealed a residual error of 1.3% and thus underscores the applicability of the model. This new biosorbent exhibited a remarkable affinity for the heavy metal ion and compared well to other reported biosorbents in the literature.

**Keywords:** banana floret, biosorption, heavy metal, artificial neural network, genetic algorithm

---

## 1. Introduction

Increased pollution resulting from excessive industrialization, urbanization, waste incineration and agricultural activities continues to magnify environmental contamination by heavy metals

---

[1]. Various technologies have been used for the removal of heavy metals including filtration, chemical precipitation, ion exchange, electrodeposition, membrane processes and adsorption using activated carbon [2]. Biosorption of heavy metals has attracted much attention recently due to its simplicity, efficiency, and availability of biomass and waste bioproducts [3]. Of keen interest are agricultural by-products such as peat [4], coconut shell [5], wood [6], banana trunk [7], rice husk [8], peanut shells [9], guava leaves [10] and banana stem [11]. A survey of the literature showed that no work had been reported on the use of banana floret as a biosorbent. In this study, Cu(II) is used as a model metal ion to assess the biosorptive potential of banana floret.

Kinetic and equilibrium studies are critical to determining the applicability of biosorbents as well as for the successful design of biosorption systems. These analyses provide an indication of sorption capacity, mechanisms as well as give some insight into the affinity of the biosorbent for the metal ion species [12]. Additionally, the development of predictive models can save time and improve efficiency in experimentation and enable the effectual upgrade to full-scale systems [13].

The objectives of this study are: (i) to determine the biosorption efficiency of banana floret as a new biosorbent; (ii) to elucidate the transport and attachment mechanisms of biosorption through batch kinetic, equilibrium, thermodynamic and desorption studies; and (iii) through single-variable kinetic and equilibrium analysis and ANN-GA modeling simulate batch process, which will enable process design and upscaling.

## 2. Materials and methods

### 2.1. Preparation of the biosorbent

Batch biosorption experiments were conducted using banana flower. The flower was first dried at 378 K for 24 h, washed and separated into three fractions which comprised the bract, the floret and the stem. The fractions were subsequently crushed and sieved into different sizes. The average particle size retained on a sieve was calculated as the geometric mean of the diameter openings in two adjacent sieves in the stack. The geometric mean size (GMS) is expressed as  $(\text{diameter of upper sieve} \times \text{diameter of lower sieve})^{0.5}$  [14].

### 2.2. Determination of metal ions concentration

Stock solutions were prepared from analytical-grade copper(II) sulfate in distilled water (prepared by a Thermo Scientific Still of pH approximately 7 and conductivity  $<5 \mu\text{S/cm}$ ). Cu(II) ions were analyzed by the cuprethol method using a Shimadzu UV-1800 Spectrophotometer and verified periodically using an Analytik-Jena contra 700 AAS.

### 2.3. SEM combined with EDS analysis

The biosorbent was characterized using a scanning electron microscope (SEM) (Hitachi S-3000 N) and an energy dispersive spectroscopy (EDS) analyzer (IXRF Systems) at a voltage of

20 kV. The SEM and EDS were used to investigate the changes in the surface microstructures and the elemental composition of the biosorbent before and after biosorption.

## 2.4. Biosorption kinetics

### 2.4.1. Kinetic studies

Batch biosorption studies were conducted using the parallel method according to EPA OPPTS method 835.1230 [15]. The study of metal uptake was done in duplicate at room temperature ( $300 \pm 2$  K) with an adsorbent mass 1.0 g/L and spiked with 50 mg/L of synthetic metal ion solution. Biosorbent masses were accurate to  $\pm 0.001$  g and solution volumes to  $\pm 0.5$  ml. Identical reaction mixtures were prepared for each time interval, agitated on a mechanical shaker and removed at predetermined time intervals [16]. The banana flower was first subjected to kinetic screening. Kinetic tests revealed the stem sorbed 14% more Cu(II) ions than the bract, while the floret sorbed 44% more than the stem. Consequently, a detailed analysis was performed on the banana floret and is reported in this study.

### 2.4.2. Adsorption yield

The ratio of adsorbed metal ion concentration to the initial metal ion concentration was calculated from Eq. (1).

$$\%Adsorption = \frac{C_o - C_t}{M} * 100 \tag{1}$$

## 2.5. Equilibrium study

The effect of initial concentration was studied by equilibrating 1.0 g/L of adsorbent in synthetic Cu(II) solution of varying concentrations (within the range of 10–100 mg/L to ensure

Expression	Equation number
$RPE\% = \frac{1}{N} \sum_{i=1}^N \left[ \frac{(q_{e_i})_{pred} - (q_{e_i})_{exp}}{(q_{e_i})_{exp}} \right] * 100$	(3)
$MPSD = 100 \sqrt{\frac{1}{N-P} \sum_{i=1}^N \left[ \frac{(q_{e_i})_{exp} - (q_{e_i})_{pred}}{(q_{e_i})_{exp}} \right]^2}$	(4)
$HYBRID = \frac{100}{N-P} \sum_{i=1}^N \left[ \frac{\left( (q_{e_i})_{exp} - (q_{e_i})_{pred} \right)^2}{(q_{e_i})_{pred}} \right]$	(5)
$R^2 = \frac{\sum_{i=1}^N \left( (q_{e_i})_{exp} - q_{e_{exp, mean}} \right)^2 - \sum_{i=1}^N \left( (q_{e_i})_{exp} - (q_{e_i})_{pred} \right)^2}{\sum_{i=1}^N \left( (q_{e_i})_{exp} - (q_{e_i})_{pred} \right)^2}$	(6)
$MSE = \left( \frac{1}{N} \sum_{i=1}^N \left[ (q_{e_i})_{exp} - (q_{e_i})_{pred} \right]^2 \right)$	(7)

**Table 1.** Error functions.

maximum sorption capacity was attained) in a shaking water bath (Julabo SW23) at temperatures varying from  $300 \pm 2$  to  $328 \pm 2$  K. The concentration of metal ions on the biosorbent was determined using the following mass balance equation:

$$q_e = \frac{(C_o - C_e)}{M} * V \quad (2)$$

## 2.6. Error analysis

The goodness of fit by the various models to the experimental data was evaluated using the coefficient of determination,  $R^2$ , the Marquardt's percent standard deviation (MPSD), hybrid error function (HYBRID), mean square error (MSE) and relative percent error (RPE) and is presented in **Table 1**.

## 3. Results and discussion

### 3.1. Kinetic modeling

Kinetic simulation of banana floret biosorption was carried out using four models: Lagergren pseudo-first order (PFO) model; pseudo-second order (PSO) model; Weber and Morris intraparticle diffusion (ID) model; and the diffusion-chemisorption (DC) model.

In 1898, Lagergren developed a first-order rate equation which was subsequently described as pseudo-first order [17]. The linear and nonlinear forms are:

$$q_t = q_e(1 - \exp^{-K_{PFO}t}) \quad (8)$$

and

$$\log(q_e - q_t) = \log q_e - \frac{K_{PFO}}{2.303}t \quad (9)$$

The PSO equation is represented by Eqs. (10) and (11) [18]. The model is based on PSO chemical reaction kinetics [19].

$$q_t = \frac{K_{PSO}q_e^2t}{1 + K_{PSO}q_e t} \quad (10)$$

and

$$\frac{t}{q_t} = \frac{1}{K_{PSO}q_e^2} + \frac{t}{q_e} \quad (11)$$

Weber and Morris [20] proposed that the rate of ID varies proportionally with the half power of time and is expressed as Eq. (12). If the rate-limiting step is ID, a plot of solute adsorbed against the square root of time should yield a straight line passing through the origin [20].

$$q_t = K_{id} \left( t^{1/2} \right) + c \tag{12}$$

The DC kinetic model was developed to simulate sorption of heavy metals onto heterogeneous media [21]. It is based on the assumption that both diffusion and chemisorption control the biosorption process. Linear and nonlinear forms are as follows:

$$q_t = \frac{1}{\frac{1}{q_e} + \frac{t^{0.5-1}}{K_{DC}}} \tag{13}$$

and

$$\frac{t^{0.5}}{q_t} = \frac{1}{q_e} * t^{0.5} + \frac{1}{K_{DC}} \tag{14}$$

Assuming, a linear region as  $t \rightarrow 0$ , the initial rate is given as:

$$k_i = K_{DC}^2 / q_e \tag{15}$$

### 3.1.1. Linear regression

**Table 2** shows the results of the linear regression analysis. The goodness of fit was assessed using error functions presented in **Table 1**. First, the experimental data were modeled using each of the kinetic models through linear regression. The highest coefficient of determination ( $R^2 = 0.9981$ ) was produced by the PSO model. This was followed by the DC model ( $R^2 = 0.9972$ ), PFO model ( $R^2 = 0.9831$ ) and finally the ID model ( $R^2 = 0.9435$ ). The equation parameters obtained from linear regression were subsequently used to construct the theoretical

Kinetic model	Linear plot	Nonlinear plot			
	$R^2$	RPE	MPSD	HYBRID	$R^2$
	Linear regression				
PFO	0.9831	59.9038	75.6477	898.5153	0.8270
PSO	0.9981	6.7008	13.1281	21.2823	0.9743
ID	0.9435	4.8812	7.1356	7.4810	0.9864
DC	0.9972	1.6146	2.4843	0.9845	0.9981
	Nonlinear regression				
PFO		11.4339	15.1570	34.5790	0.9380
PSO		6.2754	8.3444	10.3636	0.9813
ID		12.9165	17.8090	49.6369	0.9864
DC		1.6035	2.4244	0.9607	0.9981

**Table 2.** Results of linear and nonlinear regression analysis.

nonlinear curves, i.e. the form of the curve used for system design. These nonlinear plots were then compared to the primary experimental data using the error functions (RPE, MPSD, HYBRID, and  $R^2$ ). The nonlinear  $R^2$  values in **Table 2** show the correlation of the PSO model fell off significantly ( $R^2 = 0.9743$ ) while that of the DC model and ID model improved. The other error functions also support this trend. This type of occurrence has been reported by Motulsky and Christopoulos [22], where the authors explicated that the transformation of experimental data to linear forms causes some assumptions of linear regression to be violated (e.g. distortion of the experimental error) and consequently the derived slope and intercept of the regression line are not the most accurate determinations of the parameters of a model.

### 3.1.2. Nonlinear regression

A more robust simulation was performed using nonlinear regression by the Levenberg-Marquardt algorithm. The results of this analysis were assessed using error functions which revealed that the DC model produced the highest  $R^2$  and the lowest RPE, MPSD, and HYBRID values. **Figure 1a–d** shows the comparison of the experimental data to the nonlinear plots generated by both linear regression and nonlinear regression parameters. The accuracy of the DC model is confirmed by the

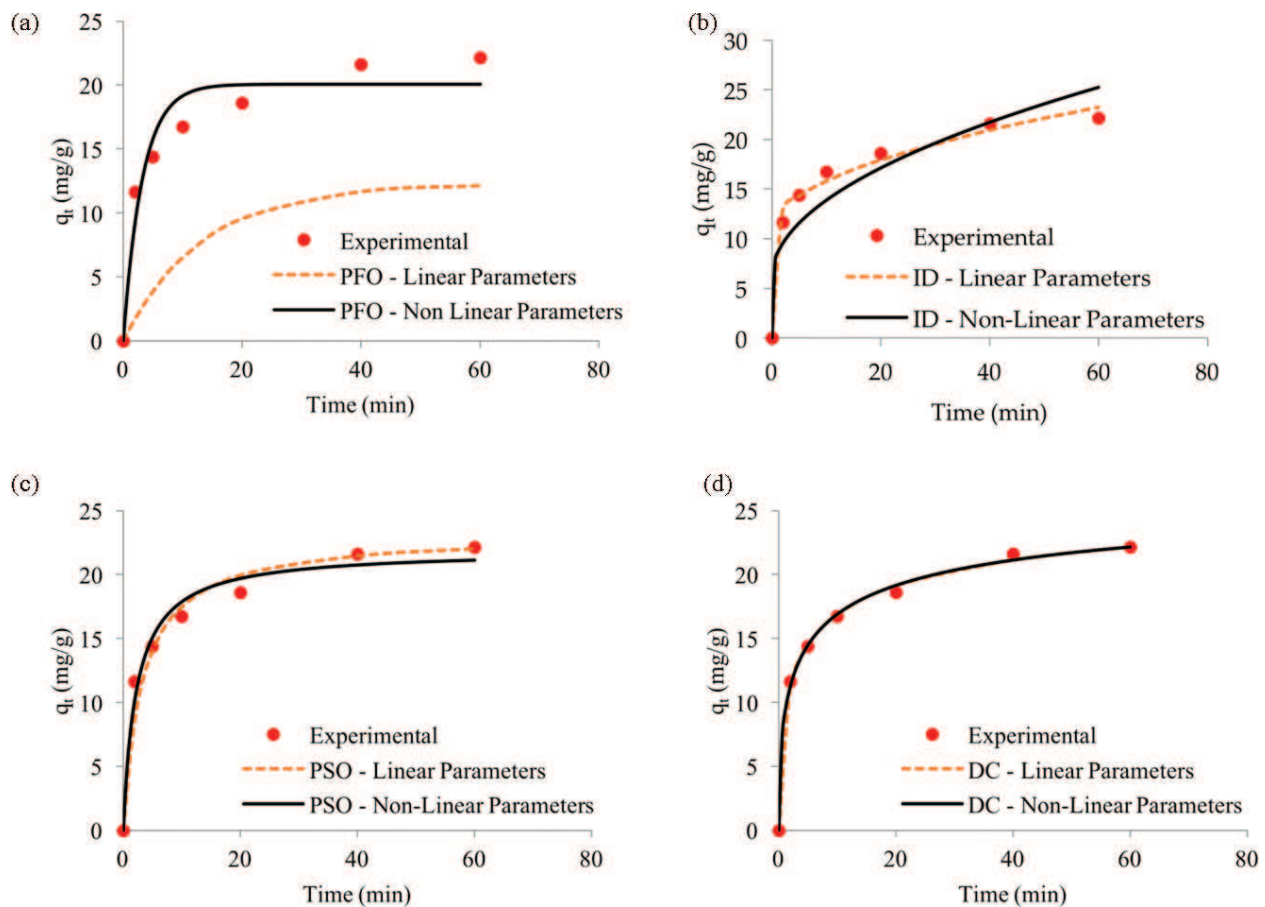


**Figure 1.** Comparison of experimental data to nonlinear kinetic curves by (a) PFO model, (b) ID model, (c) PSO model and (d) DC model.

superior simulation. What is most significant is the high precision of the DC model curves which demonstrates minimal violation as the data was transformed from linear to nonlinear forms.

### 3.2. Effect of mixing speed on biosorption

The DC model was used to assess the kinetic effect of mixing speed on the biosorption of Cu(II) onto banana floret and is presented in **Table 3**. The overall rate of biosorption increased with increasing agitation. This was expected as agitation promotes good contact between media and liquid and maintains a high-ion concentration gradient between the inner and outer regions of the particle. Further, the solvent film thickness, which surrounds the particle, reduces, and by extension, the resistance to film diffusion. This is supported by the significant increase in initial rate as agitation is increased.

### 3.3. Effect of pH on biosorption

To elucidate the impact of changing pH on biosorption, the pH was varied as presented in **Figure 2**. Maximum removal was observed at pH 5.3, followed by a significant decrease. **Figure 3** shows the results of the point of zero charge ( $pH_{PZC}$ ) of the banana floret, which was found to be 6.2. At pH values far below the  $pH_{PZC}$ , functional groups on the surface of the biosorbent become highly protonated, which can result in reduced efficiency. At pH 6.0, there exist three species,  $Cu^{2+}$  in very small quantity and  $Cu(OH)^+$  and  $Cu(OH)_2$  in large quantities [23]. The reduction in sorption observed at pH 5.6 may indicate a preference by floret for the  $Cu^{2+}$  ions over that of the other species. The maximum biosorption at pH 5.3 (below  $pH_{PZC}$ ) may in part be due to the greater preference of the higher valency  $Cu^{2+}$  ions over  $H^+$  ions.

### 3.4. Effect of particle size on biosorption

The influence of particle size was studied and is also presented in **Table 3**. It is observed that as particle size decreased, both the overall rate and the initial rate increased. The reduction in

Operational conditions	Values	Overall rate, $K_{DC}$ (mg/g-t <sup>0.5</sup> )	Initial rate $k_i$ (mg/g-t)
pH	3.2	6.4836	4.8743
	4.1	7.6858	4.1949
	5.3	13.3577	6.3379
	5.6	13.1258	9.7131
Agitation (RPM)	250	12.0172	5.0386
	350	13.3577	6.3379
	400	16.7028	9.8186
Particle, GMS (mm)	0.17	13.3873	6.3447
	0.35	11.2768	4.5407
	0.6	8.6429	3.0784

**Table 3.** DC model rate parameters for different operational conditions.

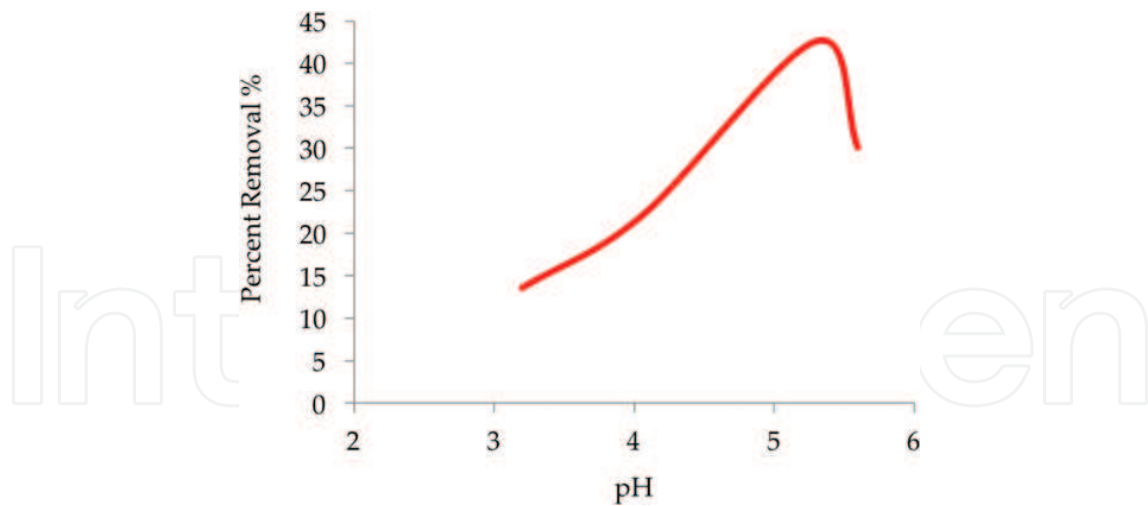


Figure 2. Effect of solution pH on Cu(II) uptake.

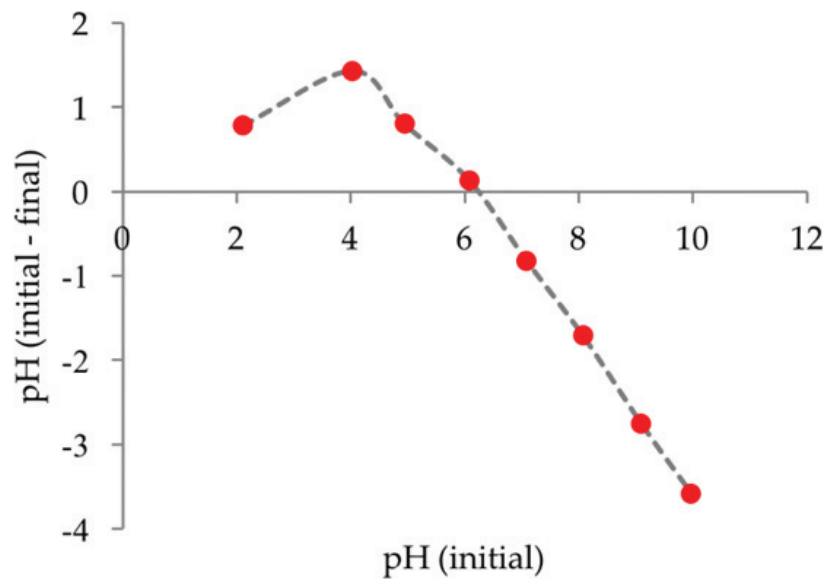


Figure 3. Point of zero charge of banana floret.

particle size is accompanied by an increase in surface area which can account for the increase in initial rate. Also, if the characteristics of the active sites on the surface of the biosorbent are the same as those within the pores, then this increase in overall rate with decreased particle size is expected.

### 3.5. Equilibrium modeling

The equilibrium capacity of banana floret for Cu(II) was assessed by nonlinear regression using two- and three-parameter equilibrium models, namely, the Langmuir isotherm, the Freundlich isotherm, the Redlich-Peterson isotherm and the Sips isotherm.

The Langmuir model (Eq. (16)) is a theoretical equilibrium isotherm originally developed to relate the amount of gas adsorbed on a surface to the pressure of the gas [24].

$$q_e = \frac{q_L K_L C_e}{1 + K_L C_e} \quad (16)$$

Firth as cited in [25], explained that the equation of the form  $x = kc^{1/n}$  was first applied to adsorption of gases by De Saussure in 1814. Its application was further extended to solutions by Boedecker in 1859 [25]. In 1906, Freundlich described the adsorption isotherm mathematically as a special case for nonideal and reversible adsorption [26]. This equation is presented as:

$$q_e = K_F(C_e)^{1/n_F} \quad (17)$$

The Redlich-Peterson isotherm (Eq. (23)) is a hybrid isotherm that incorporates the features of the Langmuir and Freundlich isotherms [27]:

$$q_e = \frac{K_{RP} C_e}{1 + \alpha_{RP} C_e^{g_{RP}}} \quad (18)$$

The Sips isotherm (Eq. (19)) is also a combined form of the Langmuir and Freundlich isotherms [28]. The model was developed for predicting heterogeneous adsorption systems [29].

$$q_e = \frac{q_S (\alpha_S C_e)^{n_S}}{1 + (\alpha_S C_e)^{n_S}} \quad (19)$$

**Table 4** shows that among the two-parameter models, the Langmuir isotherm best represented the equilibrium data. Approximately 34% increase in sorption capacity occurred as temperature was increased from 300 to 328 K. Hall et al. [30] postulated that the constant separation factor,  $R_L$ , may be used to further describe the nature of the adsorption process and to assess the suitability of the biosorbent for column applications.

$$R_L = \frac{1}{(1 + K_L C_o)} \quad (20)$$

The authors went on to explain that equilibrium conditions have an interesting effect on the shape of column breakthrough curves whereby for  $0 < R_L < 1$  (favorable equilibrium) the curve of the mass transfer zone tends to attain a constant pattern and thus become relatively self-sharpening as it advances through the column. **Figure 4** presents a plot of  $R_L$  vs.  $C_o$  for varying reaction temperatures. In all cases, the value of  $R_L$  was between 0 and 1 indicating a favorable equilibrium and by extension confirms the applicability of banana floret for column application.

Equilibrium data are also useful for batch design whereby attainable levels of treatment can be explained. Therefore, the importance of challenging the experimental data against various models and obtaining an accurate simulation cannot be overemphasized. **Table 4** shows the results of the nonlinear regression of the Redlich-Peterson and the Sips model. The Sips model produced the highest  $R^2$  among all tested equilibrium models ( $R^2$  0.9947–0.9982). According to

Models	Solution temperature (K)			
	300.15	308.15	318.15	328.15
Langmuir				
$q_L$	33.37	34.42	39.98	44.86
$K_L$	0.0526	0.0521	0.0425	0.0402
$R^2$	0.9913	0.9900	0.9883	0.9929
Freundlich				
$K_F$	4.2153	4.3226	3.9603	4.1283
$n_F$	2.2753	2.2691	2.0508	1.9877
$R^2$	0.9575	0.9572	0.9607	0.9679
Redlich-Peterson				
$K_{RP}$	1.3514	1.3783	1.2902	1.3398
$a_{RP}$	0.0110	0.0106	0.0052	0.0037
$g_{RP}$	1.2948	1.3024	1.4153	1.4750
$R^2$	0.9962	0.9949	0.9937	0.9981
Sips				
$q_s$	28.06	28.86	32.12	37.43
$a_s$	0.0756	0.0749	0.0663	0.0585
$n_s$	1.4127	1.4226	1.4622	1.3098
$R^2$	0.9974	0.9962	0.9949	0.9982

Table 4. Biosorption isotherm constants for various temperatures.

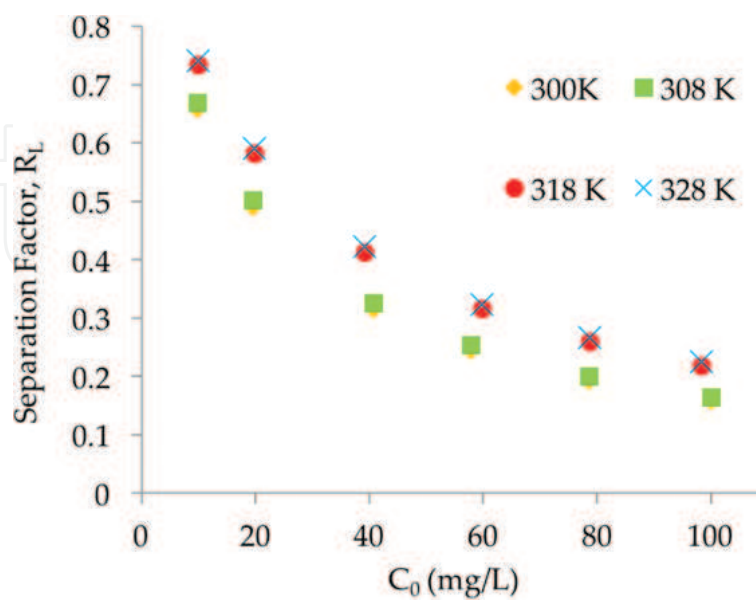


Figure 4. Variation in separation factor.

the Sips isotherm, banana floret exhibited a maximum adsorption capacity of 28.06 mg/g. This compared well with other biosorbents reported in the literature including peanut shells [31], Irish peat moss [32] and the fungal biomass *Cladosporium cladosporioides* [33] and banana stem [11], which exhibit capacities of 25.39, 17.6, 19.5 and 19.7 mg/g, respectively.

### 3.6. Thermodynamic studies

Thermodynamic effects were assessed at four different temperatures (300, 308, 318, and 328 K). Parameters such as standard Gibb’s free energy change ( $\Delta G^\circ$ ), enthalpy change ( $\Delta H^\circ$ ) and entropy change ( $\Delta S^\circ$ ) were calculated using Eqs. (21) and (22) [34]:

$$\Delta G^\circ = -RT \ln K_d \tag{21}$$

The following form of the van’t Hoff equation was applied whereby  $K_d$  is the distribution coefficient under equilibrium conditions calculated from the relationship ( $q_e/C_e$ ).

$$\ln (K_d) = \frac{\Delta S^0}{T} - \frac{\Delta H^0}{RT} \tag{22}$$

**Table 5** presents the results of the thermodynamic analysis. The  $\Delta G^\circ$  values for the range of temperature and concentration were negative, indicating a spontaneous feasible reaction and varied from  $-12.39$  to  $-7.75$  kJ/mol. Values of  $\Delta G^\circ$  lower than  $-20$  kJ/mol signify the involvement of physisorption in the biosorption process [35]. Oepen et al. as cited in [34], highlighted that the association of energy ( $\Delta H^\circ$ ) are as follows: van der Waals interactions (4–8 kJ/mol); hydrophobic bonding (4 kJ/mol); hydrogen bonding (2–40 kJ/mol); charge transfer, ligand-exchange and ion bonding (40 kJ/mol); direct and induced ion-dipole and dipole-dipole interactions (2–29 kJ/mol). In this study,  $\Delta H^\circ$  ranged from 1.5 to 9.38 kJ/mol, and consequently, the involvement of one or all of these mechanisms of attachment cannot be discounted.

The negative values of  $\Delta H^\circ$  are indicative of an exothermic sorption process. The positive  $\Delta S^\circ$  reveals increasing randomness at the solid/liquid interface during sorption or structural changes among the active sites of the biosorbent. The values of activation energy,  $E_a$ , varied according to initial concentration and ranged from 3000 to 94,000 kJ/mol. As initial concentration increases,  $E_a$

$C_o$ (mg/L)	$\Delta H^\circ$ (kJ/mol)	$\Delta S^\circ$ (kJ/mol/K)	$\Delta G^\circ$				$E_a$ (kJ/mol)	$S^*$
			300 K	308 K	318 K	328 K		
10	-5.1147	0.0529	-10.84	-11.19	-11.45	-12.39	93.6905	0.2073
20	-1.5114	0.0399	-10.51	-10.78	-11.06	-11.66	52.0972	0.1863
40	-3.6217	0.0459	-10.13	-10.54	-11.02	-11.42	26.0112	0.1867
60	-8.7953	0.0597	-9.16	-9.54	-10.15	-10.82	15.5156	0.2086
80	-8.6914	0.0565	-8.38	-8.66	-9.19	-9.96	10.2670	0.2364
100	-9.3850	0.0569	-7.75	-8.07	-8.75	-9.30	3.3152	0.1975

**Table 5.** Thermodynamic parameters.

decreases resulting in an increase in the number collision as well as an increase in reaction rate. Activation energy values between 5 and 20 kJ/mol infer physisorption is the predominant adsorption mechanism. Values greater than 20 kJ/mol and up to 40 kJ/mol generally indicate a diffusion-controlled process, and a higher value represents a reaction controlled by chemical process [36]. It can, therefore, be surmised that the mechanisms of biosorption of Cu(II) onto banana floret were significantly influenced by the initial Cu(II) concentration. The values of the sticking probability ( $S^* < 1$ ) reveal that the process was favorable.

### 3.7. Development of a predictive model

#### 3.7.1. Artificial neural network

In this study, a multilayer feed-forward backpropagation ANN model [37, 38] was developed for predicting the biosorption of copper onto banana floret. A total of 60 experimental data points was used to train and test the performance of the ANN. Each set contained four input variables comprising pH (3.2–5.6), particle size (GMS 0.17–0.06 mm), mixing speed (250–400 RPM), contact time (0–60 min), and one output variable, namely, the adsorbed concentration (4.06–23.28 mg/g). The dataset was divided into three parts, 70% for training the network, 15% for validation and 15% for testing the accuracy of the neural network model and its prediction.

The optimum architecture of the ANN was developed by first assessing the impact of 13 training backpropagation algorithms whereby the Levenberg-Marquardt algorithm produced the lowest MSE of 0.4030 and highest  $R^2$  of 0.9938. The lowest MSE and highest  $R^2$  within two training runs revealed the *Tansig* transfer function at the hidden layer and the *Tansig* transfer function at the outer layer were most optimal. A schematic representation of the architecture is shown in **Figure 5**. In this protocol, the number of neurons was varied from 2 to 20, and its

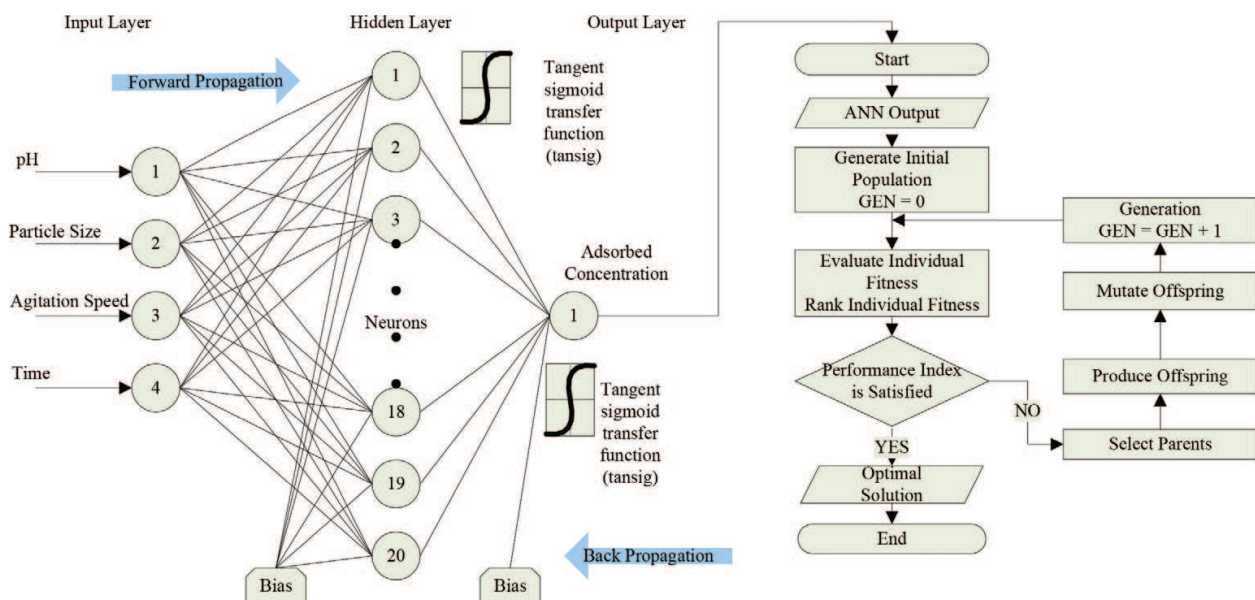


**Figure 5.** Optimized ANN-GA architecture.

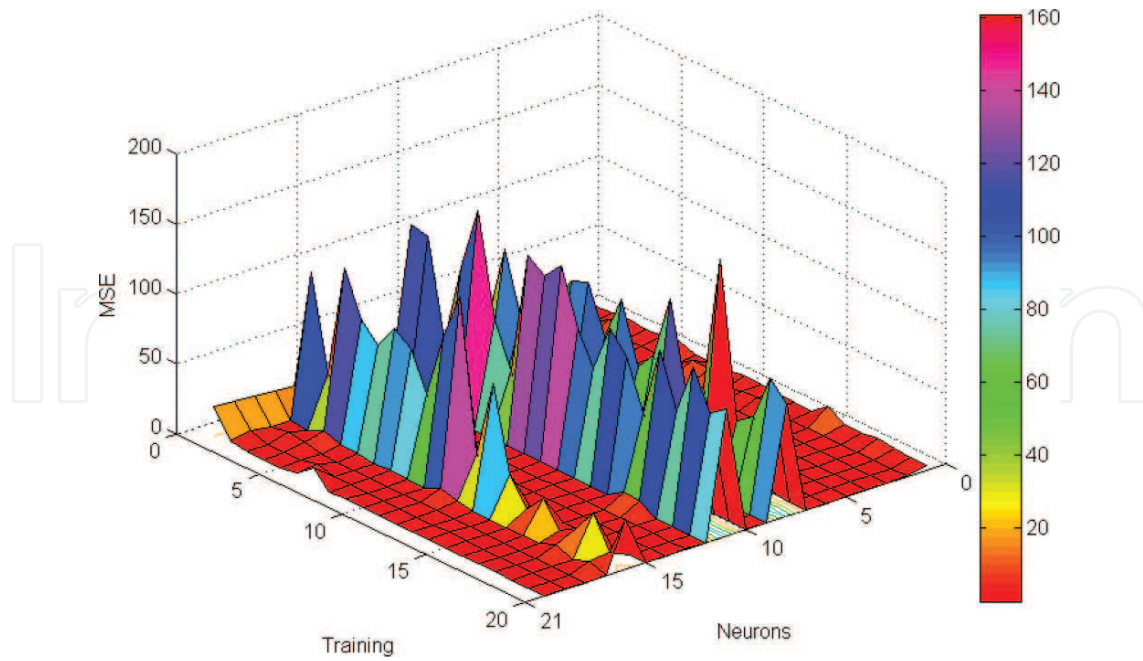


**Figure 6.** Effect of the number of neurons and training on ANN performance.

impact on performance assessed using the MSE as shown in **Figure 6**. The lowest MSE (0.0025) was obtained using 20 neurons. The figure also reveals fluctuations in MSE as the number of neurons increased. This may have resulted from the network being trapped into the local minima [39]. **Figure 7** shows a comparison of the ANN predicted data and the experimental data, which reveals a significantly high correlation ( $R^2 = 0.9972$ ) and underscores the accuracy of the ANN prediction.

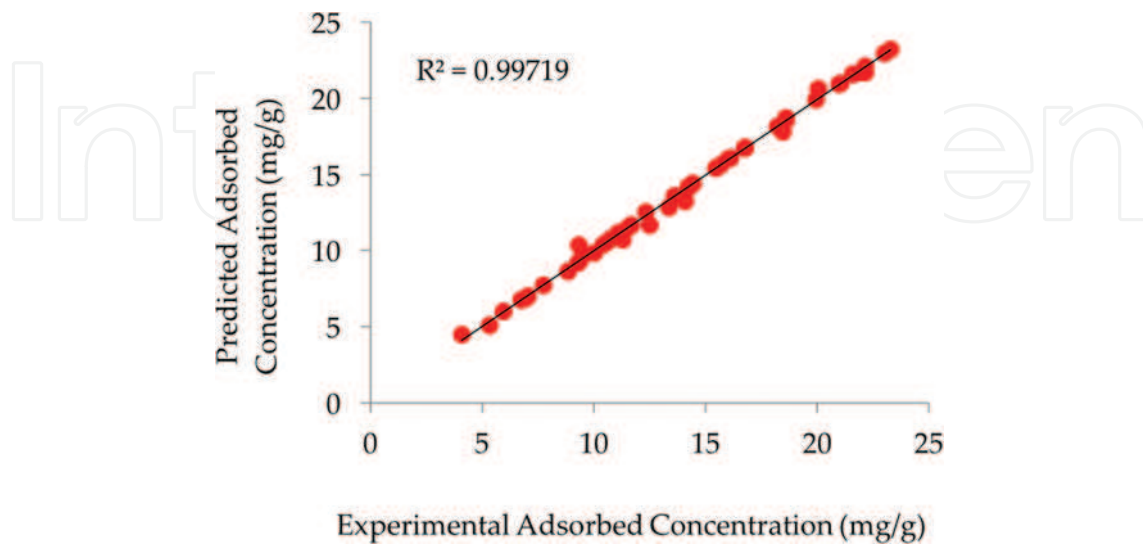


**Figure 7.** Comparison of experimental and ANN model prediction.

### 3.7.2. Formulation of empirical equation

The weights of the optimized ANN and the fitness function were used to develop an empirical expression for predicting biosorption kinetics without the ANN software using Eqs. (23), (24) and (25) [39].

$$F_i = \frac{2}{[1 + \exp(-2 * E_i)]} - 1 \quad (23)$$

where  $F_i$  is the *Tansig* transfer function used at the hidden layer. The input data are normalized in the range  $-1$  to  $1$  using Eq. (24):

$$X_{norm} = 2 \left[ \frac{X_i - X_{min}}{X_{max} - X_{min}} \right] - 1 \quad (24)$$

where  $X_i$  is the input or output variable  $X$ , and  $X_{min}$  and  $X_{max}$  are the minimum and maximum value of variable  $X$ .  $E_i$  is the weighted sum of the normalized input calculated whereby  $W_i$  represents the weights and  $bi$  is the biases and is defined as follows:

$$E_i = W_{i1} * t + W_{i2} * RPM + W_{i3} * d_p + W_{i4} * pH + bi \quad (25)$$

The predicted adsorbed concentration is therefore given by the following equation:

$$q_{t(\text{predicted})} = \frac{2}{\left[ 1 + e^{(-2 * (-1.6177F1 - 0.5105F2 - 0.4558F3 + 2.5298F4 + 1.1608F5 + 0.6342F6 - 0.7647F7 + 1.0149F8 - 0.8711F9 + 0.7553F10 - 0.2475F11 - 0.4772F12 - 0.6349F13 - 0.3057F14 + 2.2585F15 - 0.0421F16 + 1.219F17 + 1.7408F18 + 0.1456F19 + 0.2931F20 - 1.0660))} \right]} - 1 \quad (26)$$

### 3.7.3. Sensitivity analysis

A sensitivity analysis was carried out to determine the effect of each variable on the performance of the ANN model. Using the MSE and  $R^2$ , an evaluation of the performance of various possible combinations of variables was investigated [40]. The variables were combined to form four groups as presented in **Table 6**. The input variables are defined as follows:  $p1$  is time,  $p2$  is agitation,  $p3$  is particle size and  $p4$  is solution pH. The table shows  $p4$  (pH) to be the most influential parameter in the group of one variable, while  $p1$  (time) and  $p4$  (pH) were the most influential in the group of two variables, which produced the most significant improvement in the network. The greatest performance occurred with the inclusion of all four variables, which produced the lowest MSE (0.0025) and highest  $R^2$  (0.9972). Consequently, it is resolved that pH and time have the greatest influence on the ANN structure.

## 3.8. Genetic algorithm (GA) optimization

Following the development of the ANN model, the GA technique was applied using the optimization toolbox of Matlab 2012a to determine the value of the operational parameters

No.	Combination	MSE	R <sup>2</sup>
Group of one variable			
1	<i>p1</i>	11.6000	0.3264
2	<i>p2</i>	14.4100	0.1692
3	<i>p3</i>	34.9900	0.0052
4	<b><i>p4</i></b>	<b>10.2250</b>	<b>0.4445</b>
Group of two variables			
5	<i>p1 + p2</i>	8.3300	0.5329
6	<i>p1 + p3</i>	23.2000	0.2916
7	<b><i>p1 + p4</i></b>	<b>0.1900</b>	<b>0.9052</b>
8	<i>p2 + p3</i>	9.4400	0.1600
9	<i>p2 + p4</i>	7.6580	0.5476
10	<i>p3 + p4</i>	5.3254	0.5806
Group of three variables			
11	<i>p1 + p2 + p3</i>	74.2140	0.0062
12	<b><i>p1 + p2 + p4</i></b>	<b>0.2770</b>	<b>0.8879</b>
13	<i>p1 + p3 + p4</i>	1.0400	0.5184
14	<i>p2 + p3 + p4</i>	9.9110	0.5685
Group of four variables			
15	<b><i>p1 + p2 + p3 + p4</i></b>	<b>0.0025</b>	<b>0.997202</b>

**Table 6.** Performance evaluation of combinations of ANN input variables.

(pH, particle size, agitation and time) necessary for maximizing biosorption. The equation obtained from the ANN model was used as the objective function as follows [41]:

$$\text{Objective function} = \text{tansig}(LW * \text{tansig}(IW * [x(1); x(2); x(3); x(4)] + b1) + b2) \quad (27)$$

where *IW* and *b1* are the weight and bias of the hidden layer, and *LW* and *b2* are the weight and bias of output layer.

The optimized structure was achieved by a double vector population type, and the population size, population generation, crossover fraction and mutation rate were set to be 200, 100, 0.7 and 0.01, respectively. The selection, crossover and mutation operators were chosen as stochastic uniform, scattered and uniform, respectively. The fitness values versus generation are presented in **Figure 8**. The value of fitness reached to a minimum after approximately 30 generations. The ANN-GA optimization revealed that maximum removal could be obtained using pH 5.2, particle size 0.211 mm, agitation 388 rpm, and contact time 55 min. The model prediction of relative sorption capacity under these conditions was 23.25 mg/g. Laboratory experiments were subsequently conducted to validate these findings. The tests produced a

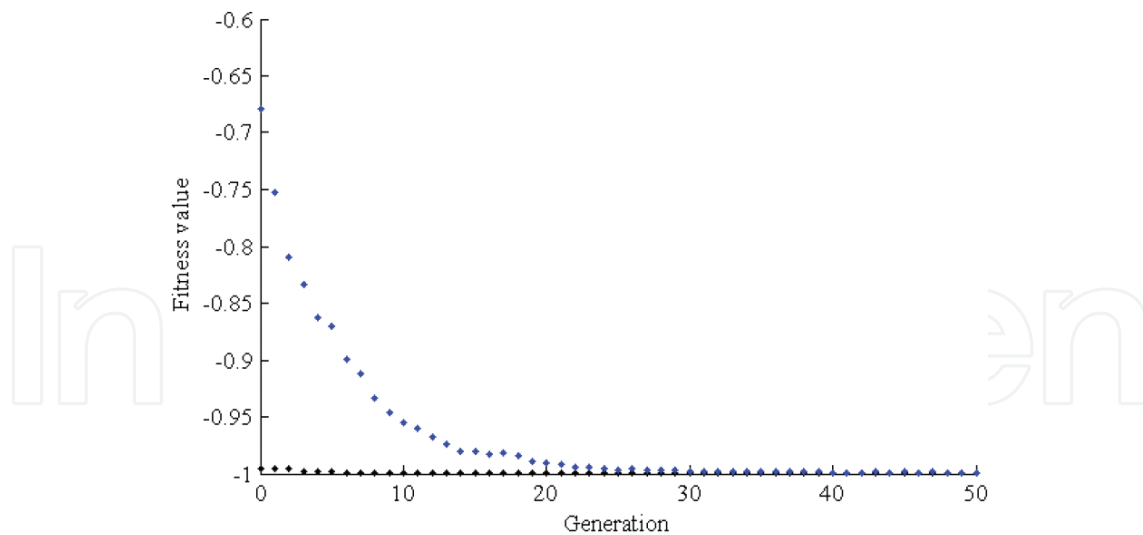


Figure 8. Fitness values versus generation.

relative sorption capacity of 22.95 mg/g, which revealed a residual error of 1.3% and therefore validate the ANN-GA structure.

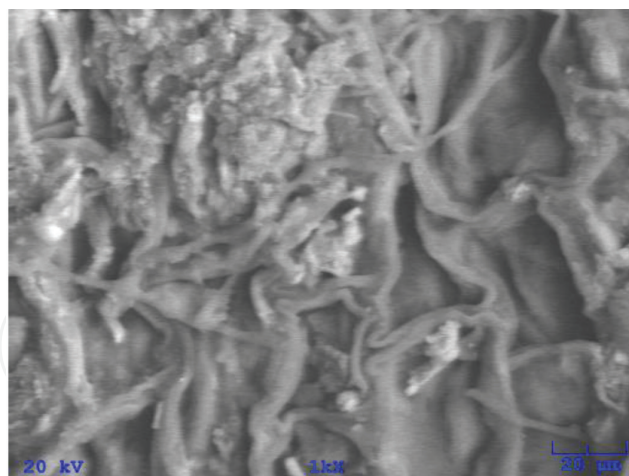
### 3.9. Elucidation of mechanisms of biosorption

#### 3.9.1. Biosorbent characteristics and performance

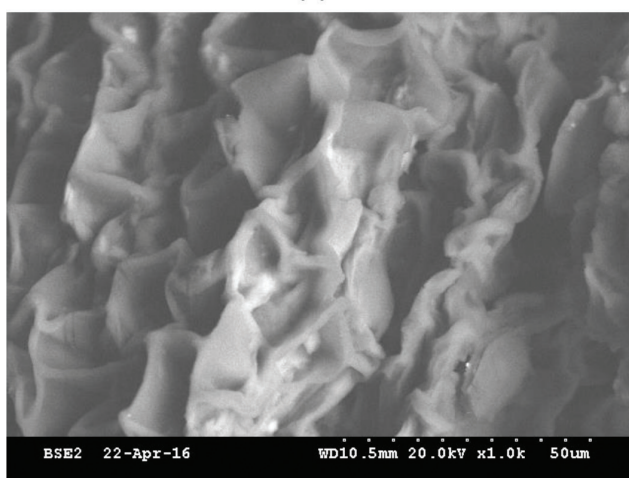
The surface morphology of floret biomass was observed by SEM before and after biosorption of Cu(II) ions (Figure 9a and b). Prior to biosorption, a rough irregular surface with a high amount of protuberance was observed. The protuberance on the biomass surface can be attributed to potassium and other salts deposition [42]. After biosorption, there was not a significant change in biomass surface morphology. However, a reduction in protuberance was observed. The EDS analysis (Figure 10a and b) reveals that banana floret contains mainly C, O and K with trace amounts of Mg, S, Si, P and Cl. After biosorption, the K, Mg and Cl peaks were removed. Similar results were reported for the biosorption of  $\text{Cr}^{3+}$  and  $\text{Pb}^{2+}$  using *Pistia stratiotes* biomass [43]. The authors explained that the adsorbate ions might have replaced some of the ions initially present in the cell wall matrix and created stronger cross-linking. The removal of K during Cu(II) biosorption may be attributed to ion exchange [44]. The appearance of a Cu peak after biosorption confirms that Cu(II) was successfully sorbed onto floret.

#### 3.9.2. Desorption using various eluents

The desorption performance of a material can aid in assessing its reuse applicability, metal recovery potential and provide some valuable insight related to the mechanism of biosorption. The desorbing solutions selected were distilled water, 0.1 M EDTA, 0.1 M HCl and 0.1 M  $\text{CaCl}_2$ . The distilled water wash revealed only 1% of the Cu(II) was weakly bound by physical forces. The secondary ion exchange cation,  $\text{Ca}^{2+}$ , recovered 11% of the sorbed ions after 60 min. The chelating agent, EDTA, known to form soluble complexes with metals ions [45] recovered



(a)



(b)

**Figure 9.** SEM micrograph of banana floret (a) before Cu(II) biosorption and (b) after Cu(II) biosorption.

60% of the sorbed ions. The harsh HCl wash, which is capable of destroying surface functional groups, released 87% of the sorbed ions after 60 min. Consequently, ion exchange and chemical bonding are confirmed attachment mechanisms of Cu(II) binding to banana floret.

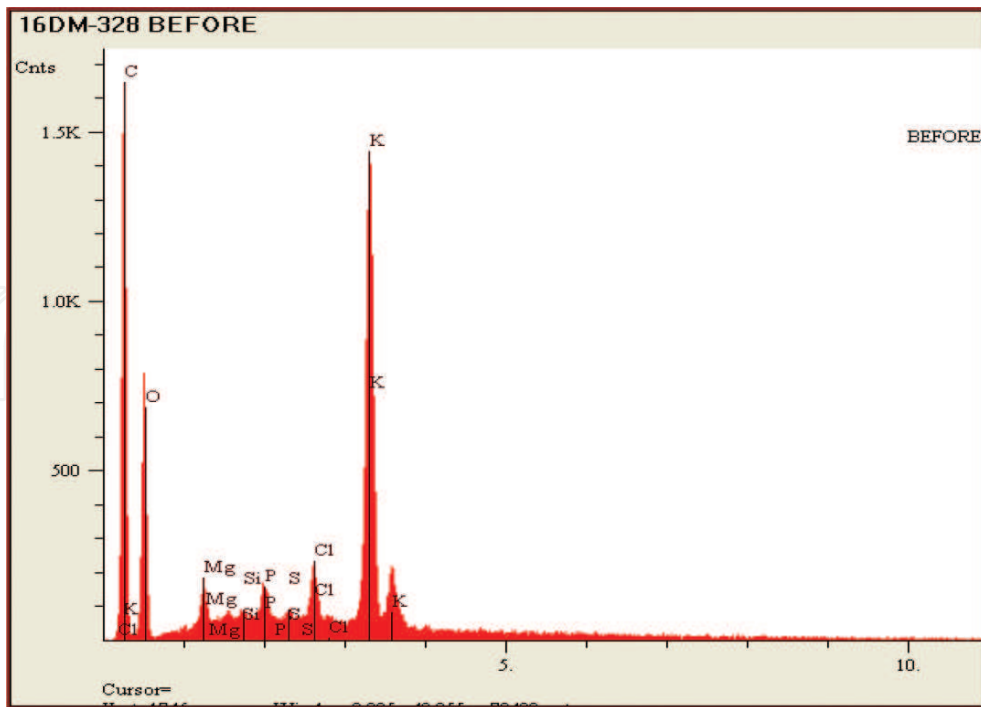
### 3.9.3. Mass transfer studies

Mass transfer studies were conducted using the external film diffusion model, the intraparticle diffusion model and the particle diffusion model.

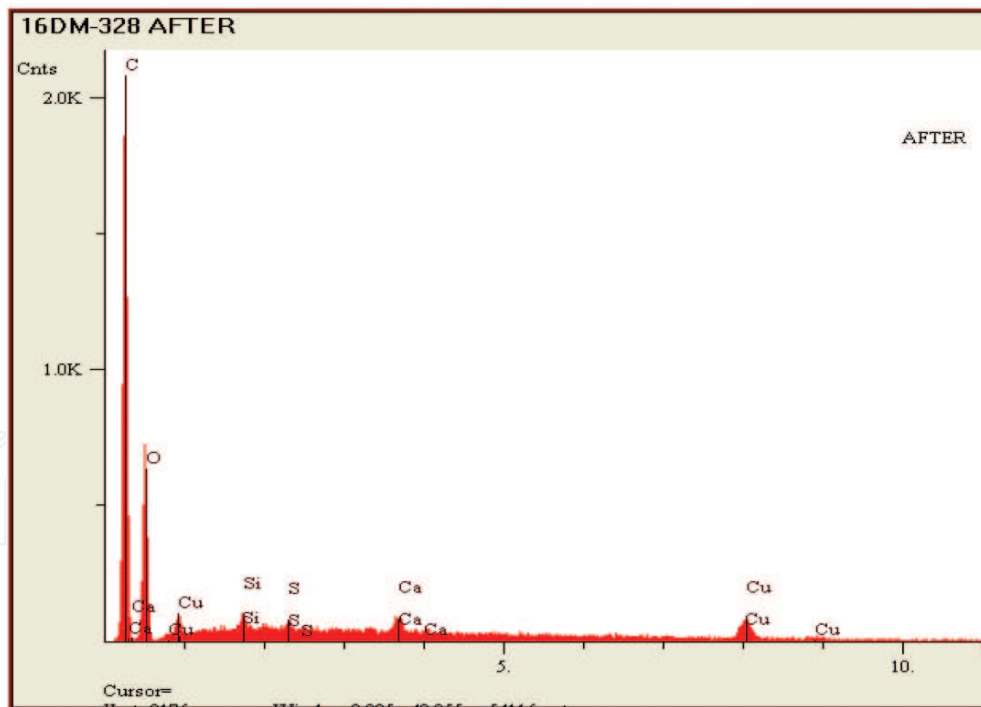
The external mass transfer model is expressed as [46]:

$$\frac{dq}{dt} = -k_f S_o (C - C_i) \quad (28)$$

Since  $C_i$  approaches zero and  $C$  approaches  $C_o$ , as  $t \rightarrow 0$ , Eq. (28) becomes:



(a)



(b)

Figure 10. EDS of banana floret (a) before Cu(II) biosorption and (b) after Cu(II) biosorption.

$$\left[ \frac{d(C/C_0)}{dt} \right]_{t=0} = -k_f S_0 \quad (29)$$

where

$$S_0 = \frac{6m_s}{d_p \rho (1 - \epsilon_p)} \quad (30)$$

The particle diffusion is described by Boyd et al. [47]:

$$X(t) = 1 - \frac{6}{\pi^2} \sum_{Z=1}^{\infty} \frac{1}{Z^2} \exp \left[ \frac{-Z^2 \pi^2 D_e t}{r^2} \right] \quad (31)$$

where  $X(t)$  is the fractional attainment at time  $t$ , given by:

$$X(t) = \frac{q_t}{q_e} \quad (32)$$

Vermeulen's [48] approximation of Eq. (31) is given as:

$$X(t) = \left[ 1 - \exp \left[ -\frac{\pi^2 D_e t}{r^2} \right] \right]^{\frac{1}{2}} \quad (33)$$

A linear plot of  $\ln[1/1 - X^2(t)]$  vs.  $t$  enables  $D_e$  to be calculated [49]:

$$\ln \left[ \frac{1}{1 - X^2(t)} \right] = \frac{\pi^2}{r^2} D_e t \quad (34)$$

The Biot number ( $Bi$ ) is given by [50]:

$$Bi = \frac{k_f r}{D_e} \quad (35)$$

A plot of  $q_t$  versus  $t^{0.5}$  in accordance with the Weber and Morris model for two sorbent sizes, namely, GMS 0.17 and 0.6 mm is shown in **Figure 11**. As the particle size decreased (which accompanies an increase in surface area and a reduction in pore length), the plots move further from the origin. Such deviation from the origin infers that intraparticle transport is not the only rate-limiting step [51].

The plot of 0.17 mm GMS reveals two distinct slopes. The first slope, which occurs within the first 30 min of the reaction, reveals the impact of intraparticle diffusion. Some researchers have

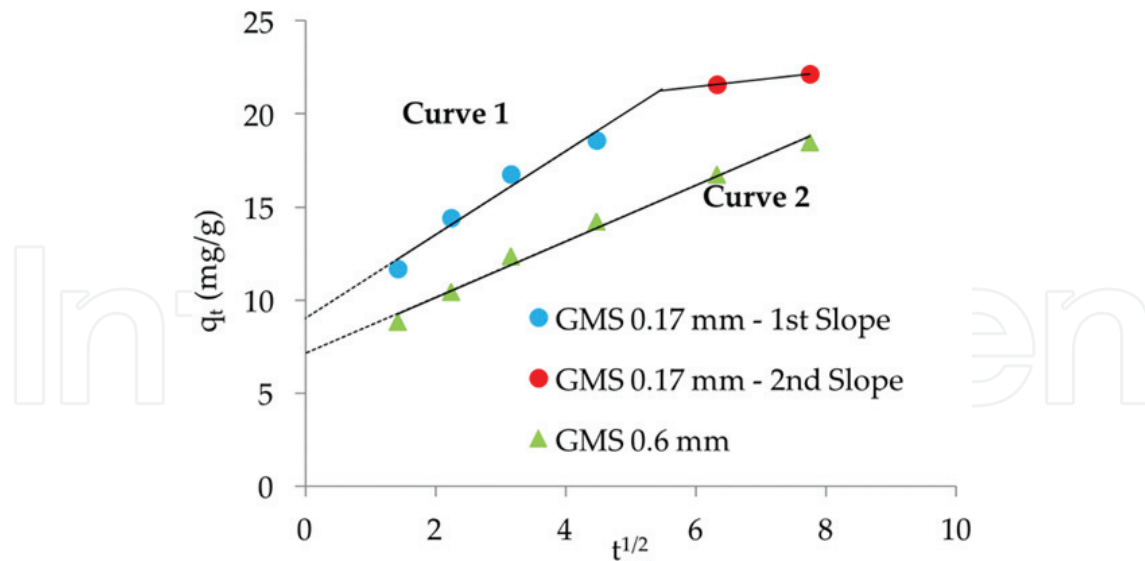


Figure 11. Kinetic plot of ID model for various particle size.

reported that the final slope corresponds to the slowing of the reaction, possibly due to a reduction in concentration gradient as the reaction approaches equilibrium [52, 53]. The plot of 0.6 mm GMS depicts the dominance of intraparticle diffusion for most of the reaction.

In order to explicate the degree of involvement of external and intraparticle diffusion, the resulting mass transfer coefficients obtained from the external and particle diffusion models were used to calculate the  $Bi$ . For  $Bi$  values  $<1.0$ , external mass transfer dominates while for  $Bi > 30$ , surface diffusion controls and for values between 1 and 30, both external and intraparticle mass transfer rates contribute [54]. The results presented in **Table 7** confirm that within the range of particle sizes studied both external and intraparticle mass transfer rates contribute to the adsorption rate. Further, as particle size increased, particle diffusivity also increased while the film diffusion coefficient decreased.

### 3.10. Design of batch biosorption system from isotherm data

Laboratory-scale equilibrium studies are used to predict batch adsorber size and performance. **Figure 12** shows the schematic of a single-stage batch adsorber with a solution volume of  $V$  (L) and the initial Cu(II) concentration,  $C_0$  is reduced to  $C_t$  as the reaction proceeds. The Cu(II) loading on the adsorbent in the reactor of mass  $M$  (g) changes from  $q_0$  to  $q_t$  with increased reaction time. The mass balance for the reactor is given by the following [55, 56]:

$$V(C_0 - C_t) = M(q_t - q_0) = Mq_t \quad (36)$$

The adsorption process at 300 K was best represented by the Sips isotherm, thus the mass balance under equilibrium condition ( $C_t \rightarrow C_e$  and  $q_t \rightarrow q_e$ ) is arranged as follows:

$$\frac{M}{V} = \frac{C_0 - C_e}{q_e} = \frac{C_0 - C_e}{\frac{q_s(\alpha_s C_e)^{n_s}}{(1 + (\alpha_s C_e)^{n_s})}} \quad (37)$$

**Figure 13** presents a series of plots of the predicted values of  $M$  (g) versus  $V$  (L) for 60, 70, 80 and 90% Cu(II) ion removal at the initial concentration of 50 mg/L and 300 K. As an example, the mass of adsorbent required for 60% Cu(II) removal from aqueous solution was 10 and 15 g,

GMS (mm)	$k_f$ (cm/min)	$R^2$	$D_e$ (cm <sup>2</sup> /min)	$R^2$	$Bi$
0.17	6.44E-03	0.8332	5.40E-5	0.9751	10.1454
0.35	1.65E-02	0.8995	1.72E-04	0.9609	16.8203
0.6	2.14E-02	0.9241	4.35E-04	0.9573	14.7441

**Table 7.** Mass transfer coefficients and  $Bi$  for the biosorption of Cu(II).

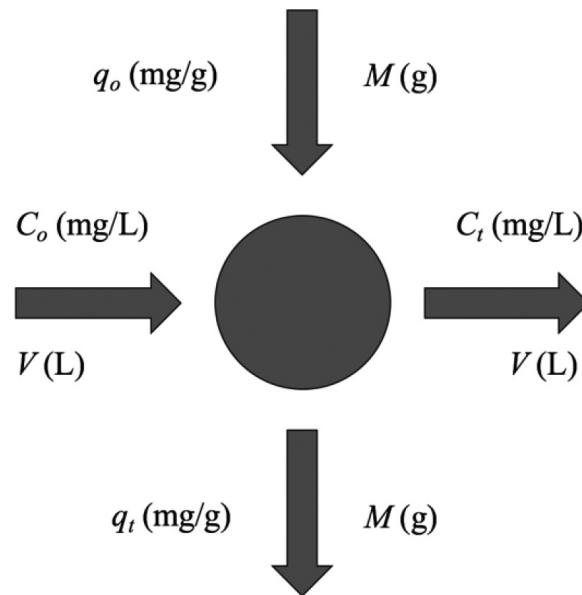


**Figure 12.** Design of single-stage batch system for Cu(II) biosorption.

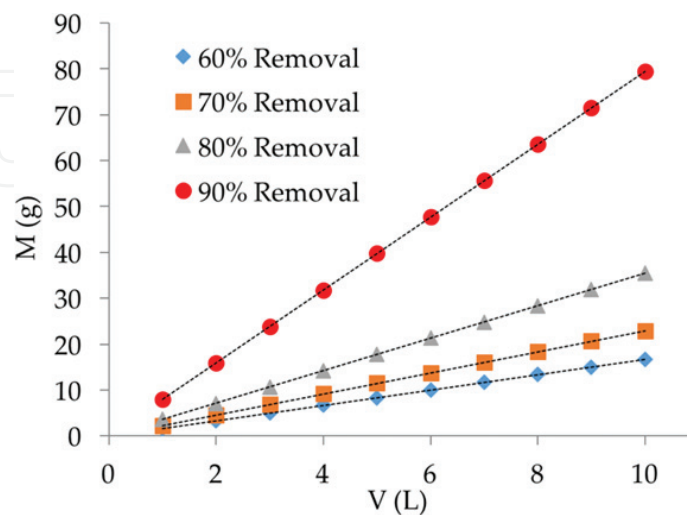


**Figure 13.** Biosorbent mass ( $M$ ) versus volume of Cu(II) solution treated ( $V$ ).

for Cu(II) solution volumes of 6 and 9 L, respectively. This evaluation becomes relevant for pilot-batch system design as well as large-scale batch applications.

## 4. Conclusion

The adsorption performance of banana floret was assessed as a new biosorbent for heavy metal removal. Cu(II) was used as a model heavy metal. Banana floret exhibited a maximum adsorption capacity of 28.06 mg/g which compares well to biosorbents reported in the literature. Operational parameters were varied and analyzed using a series of kinetic and equilibrium models. Nonlinear regression produced a more robust simulation of the kinetic data which best followed the DC model. Equilibrium data were best simulated using the three-parameter Sips isotherm. Mass transfer studies indicated that both film and intraparticle diffusion were responsible for the transport of Cu(II) to biosorption sites, while ion exchange and chemisorption were the most influential attachment mechanisms. A predictive model was successfully developed using ANN and optimized using GA. The accuracy of the ANN-GA prediction was validated by laboratory experiments, which revealed a residual error of 1.3% and therefore highlights the applicability of the model.

## Nomenclature

$a_s$	Sips affinity constant
$C$	uniform concentration of the solute in the bulk of the liquid (mg/L) (Eq. 28)
$C_e$	equilibrium concentration in solution (mg/L)
$C_i$	concentration of the solute at the particle/liquid interface (mg/L) (Eq. 28)
$C_o$	initial metal ion concentration (mg/L)
$C_t$	concentration of metal ion at any time (mg/L)
$d_p$	average particle diameter (cm) (Eq. 30)
$D_e$	particle diffusion coefficient (cm <sup>2</sup> /min)
$g_{RP}$	Redlich-Peterson exponent
$k_i$	DC initial rate (mg/g-t)
$k_f$	film mass transfer coefficient (cm/min)
$K_{DC}$	DC overall rate constant (mg/g-t <sup>0.5</sup> )
$K_{id}$	ID rate constant (mg/g-t <sup>0.5</sup> )

$K_F$	Freundlich constant related to adsorption affinity (mg/g)
$K_L$	Langmuir adsorption equilibrium constant (L/mg)
$K_{PFO}$	PFO rate constant ( $\text{min}^{-1}$ )
$K_{PSO}$	PSO rate constant (g/mg-min)
$K_{RP}$	Redlich-Peterson equilibrium constant
$m_s$	mass of biosorbent particles per unit volume ( $\text{g}/\text{cm}^3$ ) (Eq. 30)
$M$	biosorbent mass (g)
$n_F$	Freundlich constant related to heterogeneity
$n_s$	Sips index of heterogeneity
$N$	the number of experimental points
$P$	number of parameters in the regression model
$q_e$	equilibrium adsorption capacity (mg/g)
$q_L$	Langmuir monolayer sorption capacity (mg/g)
$q_t$	adsorption capacity at any time (mg/g)
$R$	universal gas constant, 8.314 J/K-mol
$S_o$	surface area for mass transfer ( $\text{cm}^{-1}$ ) (Eq. 30)
$t$	reaction time (min)
$T$	absolute temperature in K
$V$	volume (L)

#### Greek symbols

$\alpha_{RP}$	Redlich-Peterson constant
$\varepsilon_p$	biosorbent porosity (Eq. 30)
$\rho$	true biosorbent solid phase density ( $\text{g}/\text{cm}^3$ ) (Eq. 30)

## Author details

Clint Sutherland\*, Abeni Marcano and Beverly Chittoo

\*Address all correspondence to: [clint.sutherland@utt.edu.tt](mailto:clint.sutherland@utt.edu.tt)

Project Management and Civil Infrastructure Systems, The University of Trinidad and Tobago, Trinidad and Tobago (WI)

## References

- [1] Zahra N, Kalim I, Mahmood M, Naeem N. Perilous effects of heavy metals contamination on human health. *Pakistan Journal of Analytical & Environmental Chemistry*. 2017;**18**(1): 1-17. DOI: 10.21743/pjaec/2017.06.01
- [2] Low KS, Lee CK, Liew SC. Sorption of cadmium and lead from aqueous solutions by spent grain. *Process Biochemistry*. 2000;**36**(1):59-64. DOI: 10.1016/S0032-9592(00)00177-1
- [3] Kelly-Vargas K, Cerro-Lopez M, Reyna-Tellez S, Bandala ER, Sanchez-Salas JL. Biosorption of heavy metals in polluted water, using different waste fruit cortex. *Physics and Chemistry of the Earth, Parts A/B/C*. 2012;**37**:26-29. DOI: 10.1016/j.pce.2011.03.006
- [4] Lee SJ, Park JH, Ahn YT, Chung JW. Comparison of heavy metal adsorption by peat moss and peat moss-derived biochar produced under different carbonization conditions. *Water, Air, & Soil Pollution*. 2015;**226**(2):2106-2116. DOI: 10.1007/s11270-014-2275-4
- [5] Acheampong MA, Pereira JP, Meulepas RJ, Lens PN. Kinetics modelling of Cu(II) biosorption on to coconut shell and Moringa oleifera seeds from tropical regions. *Environmental Technology*. 2012;**33**(4):409-417. DOI: 10.1080/09593330.2011.576705
- [6] Ofomaja AE. Intraparticle diffusion process for lead (II) biosorption onto mansonia wood sawdust. *Bioresource Technology*. 2010;**101**(15):5868-5876. DOI: 10.1016/j.biortech.2010.03.033
- [7] Yasim NS, Ismail ZS, Zaki SM, Azis MF. Adsorption of Cu, As, Pb and Zn by banana trunk. *Malaysian Journal of Analytical Sciences*. 2016;**20**(1):187-196. DOI: 10.17576/mjas-2016-2001-20
- [8] El-Said AG. Biosorption of Pb (II) ions from aqueous solutions onto rice husk and its ash. *Journal of American Science*. 2010;**6**(10):143-150
- [9] Ugwekar RP, Lakhawat GP. Recovery of heavy metal by adsorption using peanut hull. *Journal of Advanced Engineering Technology*. 2012;**3**:39-43
- [10] Ponnusami V, Vikram S, Srivastava SN. Guava (*Psidium guajava*) leaf powder: Novel adsorbent for removal of methylene blue from aqueous solutions. *Journal of Hazardous Materials*. 2008;**152**(1):276-286. DOI: 10.1016/j.jhazmat.2007.06.107
- [11] Hasanah AN, Rizkiana F, Rahayu D. Banana peels and stem (*Musa x paradisiaca* Linn.) as biosorbent of copper in textile industry wastewater. *Research Journal of Pharmaceutical, Biological and Chemical Sciences*. 2012;**3**:1171-1178
- [12] Sutherland C, Venkobachar C. Equilibrium modeling of Cu (II) biosorption onto untreated and treated forest macro-fungus *Fomes fasciatus*. *International Journal of Plant, Animal and Environment Sciences*. 2013;**3**:193-203. DOI: 10.21276/Ijpaes
- [13] Naja G, Diniz V, Volesky B. Predicting metal biosorption performance. In: STL Harrison, DE Rawlings, J. Peterson, editors. *Proceedings of the 16th International Biohydrometallurgy Symposium*; Compress Co.: Cape Town, South Africa; 2005. pp. 553-562
- [14] Pfoest H, Headley V. Methods of determining and expressing particle size. *Feed Manufacturing Technology*. 1976:512-517

- [15] U.S. Environmental Protection Agency (USEPA). Fate, transport, and transformation test guidelines. Adsorption/desorption (batch equilibrium). Washington, DC; 2008. OPPTS 835.1230
- [16] Weber WJ, Miller CT. Modeling the sorption of hydrophobic contaminants by aquifer materials—I. Rates and equilibria. *Water Research*. 1988;**22**(4):457-464. DOI: 10.1016/0043-1354(88)90040-1
- [17] Ho YS, McKay G. A comparison of chemisorption kinetic models applied to pollutant removal on various sorbents. *Process Safety and Environmental Protection*. 1998;**76**(4): 332-340. DOI: 10.1205/095758298529696
- [18] Ho YS, McKay G. Sorption of dye from aqueous solution by peat. *Chemical Engineering Journal*. 1998;**70**(2):115-124. DOI: 10.1016/S0923-0467(98)00076-1
- [19] Ho YS, McKay G. Pseudo-second order model for sorption processes. *Process Biochemistry*. 1999;**34**(5):451-465. DOI: 10.1016/S0032-9592(98)00112-5
- [20] Weber WJ, Morris JC. Kinetics of adsorption on carbon from solution. *Journal of the Sanitary Engineering Division*. 1963;**89**(2):31-60
- [21] Sutherland C, Venkobachar C. A diffusion-chemisorption kinetic model for simulating biosorption using forest macro-fungus, *fomes fasciatus*. *International Research Journal of Plant Science*. 2010;**1**(4):107-117
- [22] Motulsky H, Christopoulos A. *Fitting Models to Biological Data using Linear and Nonlinear Regression: A Practical Guide to Curve Fitting*. New York: Oxford University Press; 2004. 19 p
- [23] Das B, Mondal NK, Bhaumik R, Roy P, Pal KC, Das CR. Removal of copper from aqueous solution using alluvial soil of Indian origin: equilibrium, kinetic and thermodynamic study. *Journal of Materials and Environmental Science*. 2013;**4**(4):392-408
- [24] Langmuir I. The adsorption of gases on plane surfaces of glass, mica and platinum. *Journal of the American Chemical Society*. 1918;**40**(9):1361-1403. DOI: 10.1021/ja02242a004
- [25] Swan E, Urquhart AR. Adsorption equations. *The Journal of Physical Chemistry*. 1927; **31**(2):251-276. DOI: 10.1021/j150272a008
- [26] Freundlich HM. Over the adsorption in solution. *The Journal of Physical Chemistry*. 1906; **57**:385-471
- [27] Redlich OJ, Peterson DL. A useful adsorption isotherm. *The Journal of Physical Chemistry*. 1959;**63**(6):1024-1026. DOI: 10.1021/j150576a611
- [28] Sips R. Combined form of Langmuir and Freundlich equations. *The Journal of Chemical Physics*. 1948;**16**(429):490-495
- [29] Günay A, Arslankaya E, Tosun I. Lead removal from aqueous solution by natural and pretreated clinoptilolite: Adsorption equilibrium and kinetics. *Journal of Hazardous Materials*. 2007;**146**(1):362-371. DOI: 10.1016/j.jhazmat.2006.12.034
- [30] Hall KR, Eagleton LC, Acrivos A, Vermeulen T. Pore-and solid-diffusion kinetics in fixed-bed adsorption under constant-pattern conditions. *Industrial & Engineering Chemistry Fundamentals*. 1966;**5**(2):212-223. DOI: 10.1021/i160018a011

- [31] Witek-Krowiak A, Szafran RG, Modelski S. Biosorption of heavy metals from aqueous solutions onto peanut shell as a low-cost biosorbent. *Desalination*. 2011;**265**(1):126-134. DOI: 10.1016/j.desal.2010.07.042
- [32] Gupta BS, Curran M, Hasan S, Ghosh TK. Adsorption characteristics of Cu and Ni on Irish peat moss. *Journal of Environmental Management*. 2009;**90**(2):954-960. DOI: 10.1016/j.jenvman.2008.02.012
- [33] Pethkar AV, Kulkarni SK, Paknikar KM. Comparative studies on metal biosorption by two strains of *Cladosporium cladosporioides*. *Bioresource Technology*. 2001;**80**(3):211-215. DOI: 10.1016/S0960-8524(01)00080-3
- [34] Delle Site A. Factors affecting sorption of organic compounds in natural sorbent/water systems and sorption coefficients for selected pollutants. A review. *Journal of Physical and Chemical Reference Data*. 2001;**30**(1):187-439. DOI: 10.1063/1.1347984
- [35] Kumar R, Rashid J, Barakat MA. Synthesis and characterization of a starch–AlOOH–FeS<sub>2</sub> nanocomposite for the adsorption of congo red dye from aqueous solution. *RSC Advances*. 2014;**4**(72):38334-38340. DOI: 10.1039/C4RA05183A
- [36] Anirudhan TS, Radhakrishnan PG. Thermodynamics and kinetics of adsorption of Cu(II) from aqueous solutions onto a new cation exchanger derived from tamarind fruit shell. *The Journal of Chemical Thermodynamics*. 2008;**40**(4):702-709. DOI: 10.1016/j.jct.2007.10.005
- [37] McCulloch WS, Pitts W. A logical calculus of the ideas immanent in nervous activity. *The Bulletin of Mathematical Biophysics*. 1943;**5**(4):115-133. DOI: 10.1007/BF02478259
- [38] Werbos PJ. Backpropagation through time: What it does and how to do it. *Proceedings of the IEEE*. 1990;**78**(10):1550-1560. DOI: 10.1109/5.58337
- [39] Shahryari Z, Sharifi A, Mohebbi A. Artificial neural network (ANN) approach for modeling and formulation of phenol adsorption onto activated carbon. *Journal of Engineering Thermophysics*. 2013;**22**(4):322-336. DOI: 10.1134/S181023281
- [40] Yetilmezsoy K, Demirel S. Artificial neural network (ANN) approach for modeling of Pb (II) adsorption from aqueous solution by Antep pistachio (*Pistacia vera* L.) shells. *Journal of Hazardous Materials*. 2008;**153**(3):1288-1300. DOI: 10.1016/j.jhazmat.2007.09.092
- [41] Ghaedi AM, Ghaedi M, Pournafard AR, Ansari A, Avazzadeh Z, Vafaei A, Tyagi I, Agarwal S, Gupta VK. Adsorption of triamterene on multi-walled and single-walled carbon nanotubes: Artificial neural network modeling and genetic algorithm optimization. *Journal of Molecular Liquids*. 2016;**216**:654-665. DOI: 10.1016/j.molliq.2016.01.068
- [42] Chen JP, Yang L. Chemical modification of *Sargassum* sp. for prevention of organic leaching and enhancement of uptake during metal biosorption. *Industrial & Engineering Chemistry Research*. 2005;**44**(26):9931-9942. DOI: 10.1021/ie050678t
- [43] Lima LK, Pelosi BT, Silva MG, Vieira MG. Lead and chromium biosorption by *Pistia stratiotes* biomass. *Chemical Engineering Transactions*. 2013;**32**:1045-1050. DOI: 10.3303/CET1332175

- [44] Vieira MG, de Almeida Neto AF, Da Silva MG, Carneiro CN, Melo Filho AA. Adsorption of lead and copper ions from aqueous effluents on rice husk ash in a dynamic system. *Brazilian Journal of Chemical Engineering*. 2014;**31**(2):519-529. DOI: 10.1590/0104-6632.20140312s00002103
- [45] Olusegun AO, Oluwafemi AS. Evaluation of chelating agents for the removal of heavy metals from contaminated soil. *Global Journal of Biochemistry and Biotechnology*. 2012; **1**(2):152-156
- [46] Mathews AP, Weber W. Effects of external mass transfer and intraparticle diffusion on adsorption rates in slurry reactors. *AIChE Symposium Series*. 1977;**73**(166):91-98
- [47] Boyd GE, Adamson AW, Myers LS Jr. The exchange adsorption of ions from aqueous solutions by organic zeolites. II. Kinetics. *Journal of the American Chemical Society*. 1947; **69**(11):2836-2848. DOI: 10.1021/ja01203a066
- [48] Vermeulen T. Theory for irreversible and constant-pattern solid diffusion. *Industrial & Engineering Chemistry*. 1953;**45**(8):1664-1670. DOI: 10.1021/ie50524a025
- [49] Lao-Luque C, Solé M, Gamisans X, Valderrama C, Dorado AD. Characterization of chromium (III) removal from aqueous solutions by an immature coal (leonardite). Toward a better understanding of the phenomena involved. *Clean Technologies and Environmental Policy*. 2014;**16**(1):127-136. DOI: 10.1007/s10098-013-0610-x
- [50] Do DD. *Adsorption Analysis: Equilibria and Kinetics: (With CD Containing Computer Matlab Programs)*. London: Imperial College Press; 1998. 555 p
- [51] Badmus MA, Audu TO, Anyata BU. Removal of lead ion from industrial wastewaters by activated carbon prepared from periwinkle shells (*Typanotonus fuscatus*). *Turkish Journal of Engineering and Environmental Sciences*. 2007;**31**(4):251-263
- [52] Wu J, Yu HQ. Biosorption of 2,4-dichlorophenol from aqueous solution by *Phanerochaete chrysosporium* biomass: Isotherms, kinetics and thermodynamics. *Journal of Hazardous Materials*. 2006;**137**(1):498-508. DOI: 10.1016/j.jhazmat.2006.02.026
- [53] Aksu Z, Kabasakal E. Batch adsorption of 2,4-dichlorophenoxy-acetic acid (2,4-D) from aqueous solution by granular activated carbon. *Separation and Purification Technology*. 2004;**35**(3):223-240. DOI: 10.1016/S1383-5866(03)00144-8
- [54] Pouloupoulos SG, Inglezakis VJ. *Adsorption, Ion Exchange and Catalysis: Design of Operations and Environmental Applications*. The Netherlands: Elsevier; 2006. 305 p. DOI: 10.1016/B978-044452783-7/50004-5
- [55] McKay G, Otterburn MS, Aga JA. Fuller's earth and fired clay as adsorbents for dyestuffs. *Water, Air, & Soil Pollution*. 1985;**24**(3):307-322. DOI: 10.1007/BF00161790
- [56] Deniz F. Dye removal by almond shell residues: Studies on biosorption performance and process design. *Materials Science and Engineering: C*. 2013;**33**(5):2821-2826. DOI: 10.1016/j.msec.2013.03.009

